Proceedings of PVP2006-ICPVT-11
2006 ASME Pressure Vessels and Piping Division Conference
July 23-27, 2006, Vancoucer, BC, Canada

PVP2006-ICPVT-11-93950

CALCULATION OF STATIC AND DYNAMIC CHARACTERISTICS OF MULTI WOUNDED RADIAL FOIL BEARING BASED ON LEAKAGE FLOW INDUCED VIBRATION THEORY

Shigehiko KANEKO
Xiaoshan WU

Department of Mechanical Engineering
The University of Tokyo
Tokyo, Japan

ABSTRACT

Dynamic pressure type foil bearings are expected to serve as shaft bearings for Micro Gas Turbines (MGT). In this study, in order to establish design guidelines of radial foil bearings, dynamical modeling of multi wounded foil bearing was carried out employing leakage flow induced vibration theory. Taking frictional forces due to attached part of the foil and the protrusion, etc. into consideration, static and dynamic characteristics were analyzed to examine the performance and the stability of radial foil bearings.

INTRODUCTION

In recent years, MGT of 100kW or less are drawing close attention as power generators equipped with cogeneration features and more recently, new research trend to combine MGT with Solid Oxide Fuel Cell is being paid much attention. Under these circumstances, aerodynamic foil bearings are considered to be the best candidate for MGT due to its ease of maintenance. Although quite a number of papers [1-4,9,11] on radial foil bearings are published and such technology is actually used in auxiliary power units (APU) for aircraft, details of bearing design guidelines have not yet been clarified. In this study, firstly, we will introduce the detail of our experimental rotor system equipped with radial foil bearings and the rotor manufactured from a commercially available turbocharger. The diameter of the rotor is 20*mm* and the surface of the rotor is coated by ceramic. The radial bearing used here is composed of two elements; i.e. a housing and a multi wounded foil with projections of hemisphere on one side in the adequate interval.

Then, the rotating shaft and the foil become bearing surfaces with the bearing action generated by forming a wedged gas membrane between the bearing surfaces. The bearing radial clearance between the rotor surface and the foil is 20mm. In the experiment, we measured rotational speed and vibrations of the rotor in the radial and axial directions [8]. Secondly, multi body dynamics analyses were conducted based on leakage flow approximation [5,7] where we took inertial force of wedged gas membrane into account. In the analysis, the foil is considered as a combination of mass less beam elements, springs and discrete mass particles, where the mass of each particle and spring coefficients are calculated based on the beam model [10].

Based on the proposed method, static characteristics of the radial foil bearing were calculated providing us the information on necessary parameters for design guidelines such as load capacity and bearing stiffness parameter. Subsequently, taking the frictional forces acting between the foil and the protrusions into consideration, equations of motion of the system are obtained by formulating fluid dynamic forces and moments acting on the rotor and the foil, yielding an eigenvalue problem.

Finally, the stability diagram showing the relation between the bearing number and mass ratio is first obtained with a multi wounded radial foil bearing.

EXPERIMENT

Radial Foil Bearing

The layout of the manufactured radial foil bearing is shown in Figure 1. This bearing is composed of two elements; i.e. a housing and a foil with projections of hemisphere on one side in the adequate interval. The foil is made from a phosphor bronze

plate of 0.1*mm* in thickness, 20*mm* in width, 202*mm* in length with many hemispherical projections whose height is 0.2*mm*.

This plate is manufactured by wet etching process and projections are made by specially designed jig. When installing the foil to the housing, the plate was bent at the position of 3*mm* measured from the edge of the plate. Then, the foil was wounded triply and fixed with the housing. Due to the rotation of the shaft, a wedge like space with high pressure is yielded between the shaft and the inner bearing surface, which levitates the rotating shaft. The bearing clearance is represented as C and is described by the equation as follows:

$$C = \left(D - d\right)/2 - 2h - 3t \qquad (1)$$

where C , D , d , h and t denotes radial clearance, inner diameter of housing, diameter of rotor, height of projections and thickness of the foil, respectively. The bearing radial clearance between axial surface and bearing surface is 20μm, because the foil is triply wounded.

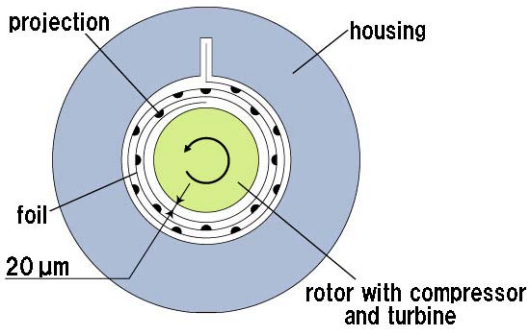

Figure 1 Schematic view and composition of radial foil bearing

These types of multi wounded foil bearing have advantages of easy fabrication and assemble compared with usual air bearing. In Figure 2, dimensions and compositions of the foil employed in the experiment are illustrated which has another advantage of changing bearing characteristics by just accommodating the density and distribution pattern of the projections.

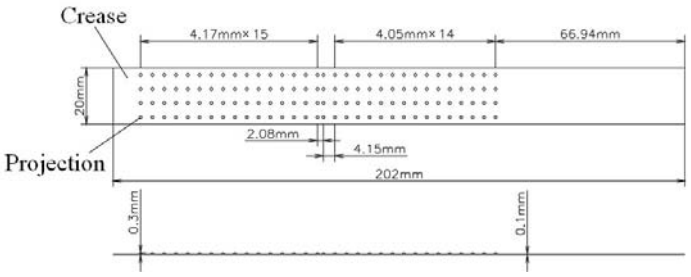

Figure 2 Radial foil with projections

In Figure 3, enlarged sketch of a projection is shown. The thickness of the foil is 0.2*mm* and the height of a hemispherical projection formed by specially designed jig is 0.2*mm*.

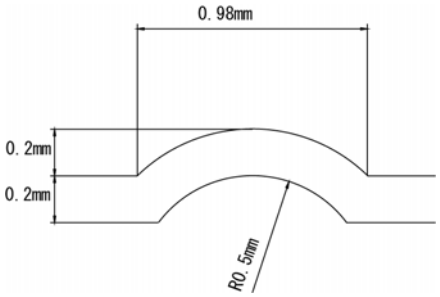

Figure 3 Enlarged projection

Experimental Setup

The composition of the rotor and rotor housing used in the experiment is shown in Figure 4. The rotating shaft, the weight of which is 0.5*kg* consists of the following four parts, the rotor with a turbine, a sleeve, a thrust disk and a nut for fixing the thrust disk to the rotor and the shaft is supported by two radial foil bearings and a spiral thrust bearing. The martensitic stainless steel was selected as a material of the sleeve, and the surface of the shaft is coated by ceramic. At the right end of the rotating shaft, a reverse thread was cut to fix the thrust disk and a through hole was drilled for measuring the rotational speed. The sleeve was inserted under pressure and fixed with the shaft.

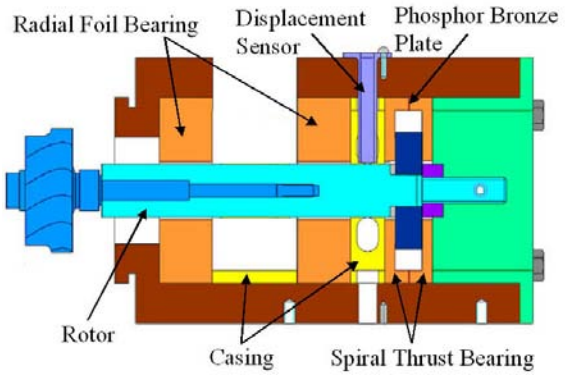

Figure 4 Experimental apparatus

MODELING PROCUDURE

Modeling of Radial Foil Bearing

To make mathematical model of the foil bearing, we expanded the foil as Figure 5(a) where flow runs through the narrow passage between the surface of the inner foil and the surface of the rotating shaft due to the rotation of the shaft.

Then, we introduce the idea that the deformation of projections on the expanded foil plays as a linear spring element as shown in Figure 5(b).

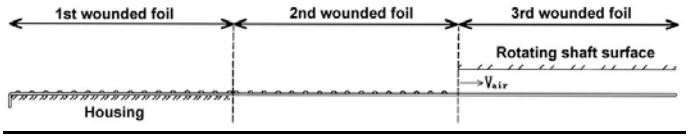

Figure 5(a) Modeling radial foil with projections

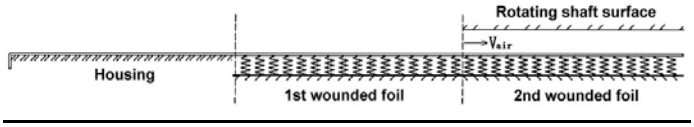

Figure 5(b) Modeling radial foil with projections

For further simple modifications, we combine the spring element corresponding to the first and second wounded foil as single spring element as shown in Figure 5(c).

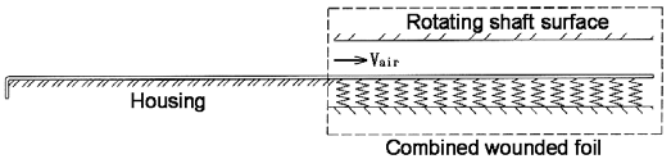

Figure 5(c) Modeling radial foil with projections

In what follows, we will make mathematical model with the area surrounded by the dashed line in Figure 5(c) which means the target system is composed of a flexible cantilevered plate supported by discrete linear springs with the flow running on the upper surface of the plate.

Mathematical modeling

As a next step, we introduced the idea of multi body dynamics that the flexible foil can be regarded as a discrete beam model consisting of n mass particles, dampers and rotational springs, where ℓ_i and ϕ_i denote respectively, the length of a beam element and rotational angle measured relative to the x-axis, and we chose $\ell = \ell_1 = \ell_2 = \cdots = \ell_n = 2\pi R/n$ (constant) where R denotes average radius of the wounded foil. Due to the rotation and the vibration of the shaft, the upper wall in Figure 6 moves at the velocity of U and V.

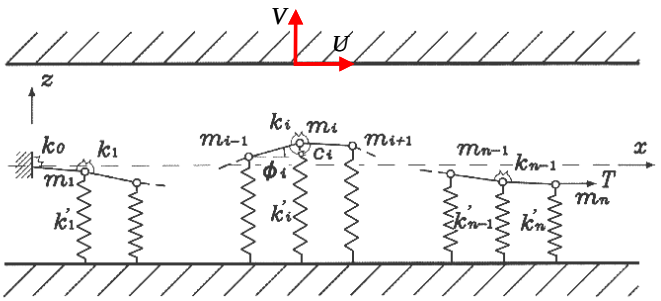

Figure 6 Multi body dynamical modeling

ANALYSIS OF STATIC CHRACTERISTICS

Steady fluid force and foil deformation

The flow in a passage of length ℓ and height h shown in Figure 7 is discussed. The flow is assumed to be two dimensional, incompressible and viscous. Starting the continuity and Navier-Stokes equations for the flow, we will derive another type of governing equation as

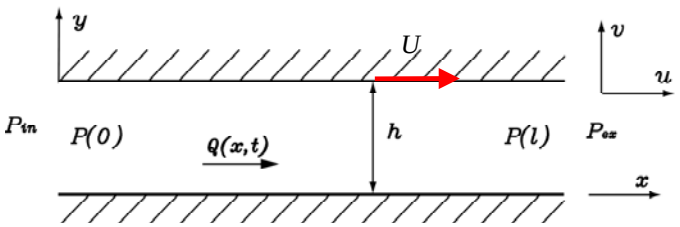

Figure 7 Leakage flow model

$$\frac{\partial Q}{\partial x} - U\frac{\partial h}{\partial x} + V = 0 \tag{2}$$

$$\frac{\partial Q}{\partial t} + \frac{\partial}{\partial x}\left(\frac{Q^2}{h}\right) = -\frac{h}{\rho}\frac{\partial P}{\partial x} - \frac{12\nu U}{h} \tag{3}$$

where Q, ρ, P, h, ν, U, V denote volumetric flow rate, density of fluid, pressure, passage height, kinematic viscosity of fluid, moving velocity of upper wall in x and z direction.

By separating the foil into n elements, corresponding center angle of each sector is $2\pi/n$ $[rad]$ and the passage height at i-th element is given by

$$\bar{h}_i \simeq c\left\{1 + \kappa\cos\left(\frac{2\pi}{n}i\right)\right\} \tag{4}$$

where c and κ denotes radial clearance and eccentricity, respectively.

Steady pressure acting on i-th element is calculated by Eqs.(2) and (3) and are expressed as

$$\bar{P}_i(x) = \left(-\frac{12\mu\bar{Q}_i}{\bar{h}_i^3} + \frac{6\mu U}{\bar{h}_i^2} \right) x + \left(-\frac{6\mu\bar{Q}_i\ell}{\bar{h}_i^3} + \frac{3\mu U\ell}{\bar{h}_i^2} \right) + \bar{P}_i\left(-\frac{1}{2}\right) \tag{5}$$

where $\bar{}$ means steady component and μ means viscosity of fluid.

In the following, we will formulate the deformation of the foil. Steady fluid force acting on i-th element is calculated by integrating the steady pressure with x and is obtained as

$$\{\bar{\mathbf{f}}_z\} = \int_{-\frac{1}{2}}^{\frac{1}{2}} \{\bar{\mathbf{P}}(x)\}\left(\frac{1}{2}+x\right)dx + \begin{bmatrix} 0 & 1 & \cdots & 0 \\ \vdots & \ddots & \ddots & \vdots \\ 0 & & & 1 \\ 1 & 0 & \cdots & 0 \end{bmatrix} \int_{-\frac{1}{2}}^{\frac{1}{2}} \{\bar{\mathbf{P}}(x)\}\left(\frac{1}{2}-x\right)dx \tag{6}$$

The deformation of i-th element is determined by the following equation

$$\{\mathbf{k}'\}\{\Delta\mathbf{h}\} = \{\bar{\mathbf{f}}_z\} \tag{7}$$

where $\{\mathbf{k}'\}$ and $\{\Delta\mathbf{h}\}$ denote stiffness due to projections and the deformation of the beam at the corresponding point.

Calculation procedure of static characteristics

First, we calculate the case without deformation and figure out the amount of deformation by Eq.(4). Then, taking account of additional deformation calculated by Eq.(7) and superimposing, we recalculate the pressure by Eq.(5). We repeat such process until sufficient convergence will be obtained.

Then, the steady fluid forces acting in the direction of eccentricity and one perpendicular to which are calculated by the following equations,

$$F_X = \sum_{i=1}^{n} \left(\int_{-\frac{1}{2}}^{\frac{1}{2}} \bar{P}_i(x)\,dx \right) \cos A_i \tag{8}$$

$$F_Y = \sum_{i=1}^{n} \left(\int_{-\frac{1}{2}}^{\frac{1}{2}} \bar{P}_i(x)\,dx \right) \sin A_i \tag{9}$$

where $A_i = \dfrac{\pi(2i-1)}{n}$.

The equilibrium relation between fluid force and the bearing load is given by

$$mg\cos\theta + F_X = 0 \tag{10}$$

$$-mg\sin\theta + F_Y = 0. \tag{11}$$

Then, we can determine load capacity of the bearing W and the eccentric angle θ as follows,

$$W = \sqrt{{F_X}^2 + {F_Y}^2} \tag{12}$$

$$\theta = \arctan\frac{F_Y}{F_X} \tag{13}$$

Calculated results

As an example, calculated results of the rotor locus and the relation between load capacity and eccentricity ratio are shown in Figures 8 and 9, where total number of the elements is 20 and load capacity shown here is non-dimensionalized by the shaft weight.

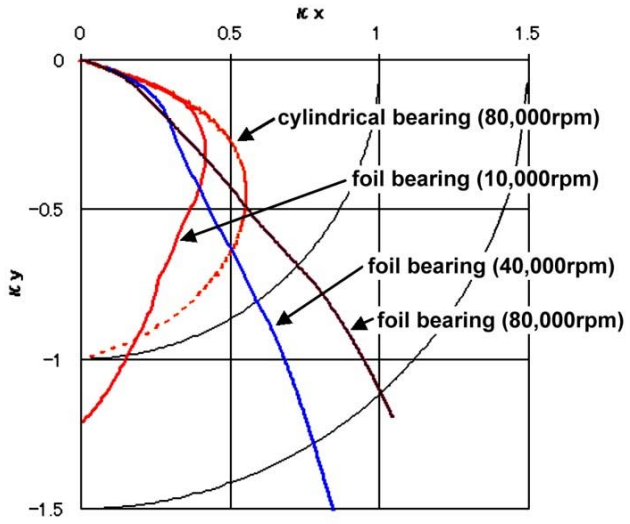

Figure 8 Rotor locus

In Figure 8, the result in the case of cylindrical bearing is also shown as a reference where gravitational force acts downward. One can find that eccentricity ratio κ becomes larger than unity in the case of foil bearing due to the deformation of the foil.

In Figure 9, we can find that load capacity in the case of foil bearing changes moderately and is affected less by the eccentricity ratio change compared with cylindrical bearing. Increasing the eccentricity ratio induces higher pressure in the gap between the foil surface and rotating shaft surface and then leads to larger deformation of the foil.

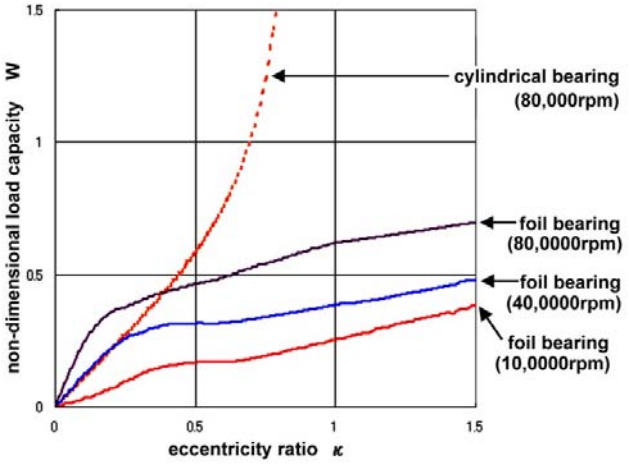

Figure 9 Relationship between κ and W

ANALYSIS OF DYNAMIC CHRACTERISTICS

Equation of motion for foil

In Figure 6, rotational spring constant k_i connecting the mass of ith element m_i and two adjacent foil elements is formulated based on the beam theory. When the moment M is acting on both sides of a small element of length ℓ , the radius of curvature of the beam r may be determined by

$$\frac{1}{r} = \frac{M}{EI}. \tag{14}$$

Substituting $r = \ell/\theta$ in Eq. (14) results in

$$\frac{M}{\theta} = \frac{EI}{\ell}. \tag{15}$$

Since the stiffness of the rotational spring is defined as $k = M/\theta$, substituting it into Eq.(15) yields

$$k = MI / \ell. \tag{16}$$

Additionally, the discrete mass equal to the mass of beam element is defined as

$$m = \rho_m \ell \tag{17}$$

where ρ_m denotes the density of the foil.

Then, the discrete mass of ith element and the stiffness of the rotational spring are finally determined as

$$m_i = \frac{1}{2}\rho_m \left(\ell_i + \ell_{i+1}\right) \tag{18}$$

$$k_i = \frac{2EI}{\ell_i + \ell_{i+1}}. \tag{19}$$

It is assumed that the damping moment acting on ith element is proportional to the difference of angular velocities of tow adjoining elements:

$$M_{c_i} = -c_i(\dot{\phi}_{i+1} - \dot{\phi}_i). \tag{20}$$

Furthermore, the position of ith particle is given from the geometrical relationship

$$x_i = \sum_{j=1}^{i} \ell_j \cos\phi_j \quad , \quad z_i = \sum_{j=1}^{i} \ell_j \sin\phi_j \ . \tag{21}$$

Then, the Lagrangian for the system becomes

$$L = \sum_{i=1}^{n} \frac{m_i}{2}(\dot{x}_i^2 + \dot{z}_i^2) - \sum_{i=0}^{n-1} \frac{k_i}{2}(\phi_{i+1} - \phi_i)^2 - \sum_{i=1}^{n} \frac{k_i'}{2} z_i^2 - T\sum_{i=1}^{n} \ell_i(1 - \cos\phi_i). \tag{22}$$

Substituting Eq.(22) into Lagrange's equation and linearization, the following equation motion is obtained:

$$[J_M]\{\ddot{\boldsymbol{\varphi}}\} + [C_M]\{\dot{\boldsymbol{\varphi}}\} + ([K] + [K'])\{\boldsymbol{\varphi}\} = \{\mathbf{Q_z}\} + \{\mathbf{Q_r}\} + \{\mathbf{Q_r'}\}. \tag{23}$$

where $\{\mathbf{Q_z}\}$, $\{\mathbf{Q_r}\}$, denote generalized forces contributed by the pressure, shearing force from the fluid and $\{\mathbf{Q_r'}\}$ denotes one from the structural damping force with frictional force due to the Column friction between the projections and a foil.

Unsteady pressure acting on the wall

In this paper, it is assumed that the motion of a discrete beam element consists of small amplitude translational and rotational motion as shown in Figure 10 under the situation that the velocity profile of the leakage flow is affected by the running speed of upper wall U.

Assuming that the height h, rotation angle θ, pressure P, and flow rate Q change with angular frequency Ω , then h, P and Q can be described as

$$h(x,t) = \bar{h} + (\Delta h + x\Delta\theta_0)e^{i\Omega t} \tag{26}$$

$$P(x,t) = \bar{P}(x) + \Delta P(x) e^{i\Omega t} \tag{27}$$

$$Q(x,t) = \bar{Q} + \Delta Q(x) e^{i\Omega t} . \tag{28}$$

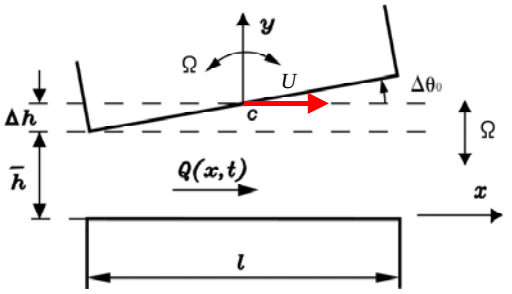

Figure 10 Translational and rotational vibration model

Substituting Eqs.(26)-(28) into Eqs.(2) and (3), linearlized unsteady pressure is formulated as a non-dimenasional form as

$$\begin{aligned} p_i(X) = &-2(i\omega + \frac{\ell\lambda}{2\bar{h}_i}) q_i (-\frac{1}{2}) X + \left\{ 4X + (i\omega + \frac{\ell\lambda}{2\bar{h}_i})(X^2 + X) \right\} i\omega\eta_i \\ &+ \left\{ (i\omega + \frac{\ell\lambda}{2\bar{h}_i})(\frac{X^3}{3} - \frac{X}{4}) + 2X^2 \right\} i\omega\Theta_i + \left\{ (\frac{3\ell\lambda}{4\bar{h}_i} - \xi) X^2 + 2X \right\} \Theta_i \\ &+ \left(\frac{3\ell\lambda}{2\bar{h}_i} - 2\xi \right) \eta_i X - \left\{ (i\omega + \frac{\ell\lambda}{2\bar{h}_i})(\frac{X^2}{4} + \frac{X}{4}) + X \right\} \frac{\bar{h}_i}{3\ell} \mathrm{Re}\,\xi\Theta_i + C_i \end{aligned} \tag{29}$$

where

$$\begin{aligned} C_i = &-(i\omega + \frac{\ell\lambda}{2\bar{h}_i} + 2\xi_{in}) q_i (-\frac{1}{2}) - \left\{ \frac{1}{2} + \frac{1}{12}(i\omega + \frac{\ell\lambda}{2\bar{h}_i}) \right\} i\omega\Theta_i \\ &+ (1 + \frac{\xi}{4} - \xi_{in} - \frac{3\ell\lambda}{16\bar{h}_i})\Theta_i + (\frac{3\ell\lambda}{4\bar{h}_i} - 2\xi + 2\xi_{in})\eta_i \\ &+ \left\{ 2 + \frac{1}{4}(i\omega + \frac{\ell\lambda}{2\bar{h}_i}) \right\} i\omega\eta_i - \left\{ \frac{1}{16}(i\omega + \frac{\ell\lambda}{2\bar{h}_i}) + \frac{1}{2} \right\} \frac{\bar{h}}{3\ell} \mathrm{Re}\,\xi\Theta_i . \end{aligned}$$

In these equations, no-dimensional quantities are defined as

$$\lambda = \frac{48}{\mathrm{Re}}, \mathrm{Re} = \frac{Q}{\nu}, X = x/\ell, q = \Delta Q/\bar{Q}, \eta = \Delta h/\bar{h}$$

$$\xi = \frac{12\nu U\ell}{\bar{Q}^2}, \Theta = \frac{\ell}{\bar{h}}\Delta\theta_0, p = \frac{\Delta P(x)}{\frac{\rho}{2}\frac{\bar{Q}^2}{\bar{h}^2}}$$

ξ_{in} : inlet pressure loss coefficient.

Fluid force acting on a foil element

In what follows, we discuss the formulation of fluid forces from the pressure. As is shown in Figure 11, when single foil element undergoes both translational and rotational oscillation with the point c, the height of the upper passage is given by Eq.(26).

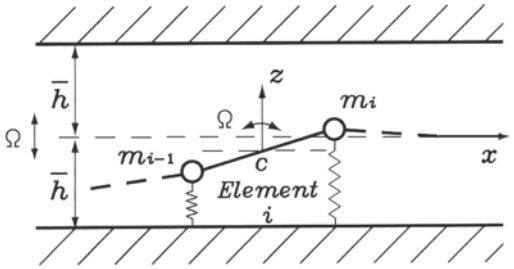

Figure 11 Motion analysis of single element

Non-dimensional pressure is describe as

$$\mathrm{P}_i(X) = \bar{p}_i(X) + p_i(X) e^{i\Omega t} . \tag{30}$$

Summation of the normalized pressure acting on ith element produces normalized forces f_{i+} and f_{i-} acting on both end of the element, which are

$$f_{i+} = \int_{-\frac{1}{2}}^{\frac{1}{2}} \mathrm{P}_i(X)(\frac{1}{2} + X) dX \tag{31}$$

$$f_{i-} = \int_{-\frac{1}{2}}^{\frac{1}{2}} \mathrm{P}_i(X)(\frac{1}{2} - X) dX . \tag{32}$$

Substituting Eq.(30) into Eqs.(31) and (32), then, fluid force is obtained as a non-dimensional form as

$$\begin{aligned} \{\mathbf{f_{fz}}\} = &\{\bar{\mathbf{f}}_{\mathbf{fz}}\} + \left(\left[J_{f11} \mid J_{f12} \mid 0 \mid 0 \right] (i\omega)^2 \right. \\ &+ \left[C_{f11} \mid C_{f12} \mid C_{f13} \mid 0 \right] (i\omega) \\ &\left. + \left[K_{f11} \mid K_{f12} \mid K_{f13} \mid K_{f14} \right] \right) \begin{Bmatrix} \{\mathbf{\Theta}\} \\ \{\mathbf{\eta}\} \\ \{\mathbf{q}(-1/2)\} \\ \{\mathbf{C}\} \end{Bmatrix} e^{i\Omega t} \end{aligned} \tag{33}$$

where $\{\mathbf{f_{fz}}\}$, $\{\mathbf{\Theta}\}$, $\{\mathbf{\eta}\}$, $\{\mathbf{q}(-1/2)\}$, $\{\mathbf{C}\}$ are the vectors denoting the fluid force vector, rotation angle vector, parallel displacement vector, fluctuating flow vector and integration constant vector, respectively. From Eq.(33), we can finally derive generalized fluid force as a dimensional vector as

$$\{\mathbf{Q}_z\} = \frac{\rho}{2}\frac{\bar{Q}^2}{\bar{h}^2}\ell^2 \cdot [L_2]\{\mathbf{f}_{fz}\}. \tag{34}$$

As in the same manner, we can formulate the effect of shear stress acting on the surface of the foil as

$$\{\mathbf{Q}_r\} = \tau\ell^2 [L_1]\{\boldsymbol{\varphi}\} \tag{35}$$

where $\tau = 6\mu\bar{Q}/\bar{h}^2 - 2\mu U/\bar{h}$.

Structural and frictional force

It is not easy to formulate structural and frictional force due to the friction between the projections and a foil properly. Therefore, in this paper, the effect is taken into account as an equivalent linear damping proportional to the velocity in the radial direction which gives us the form as

$$\{\mathbf{Q}_r'\} = \left[C_{fr}\right]\{\dot{\boldsymbol{\varphi}}\} \tag{36}$$

Equation of motion of a foil

Combining Eqs.(33)-(36) together with Eq.(23), we may write the equation motion of a foil as

$$\left(\left[\begin{array}{c|c} J_{w31} & 0 \\ \hline J_{w21} & 0 \end{array}\right](i\omega)^2 + \left[\begin{array}{c|c} C_{w31} & C_{w32} \\ \hline C_{w21} & C_{w22} \end{array}\right](i\omega) + \left[\begin{array}{c|c} K_{w31} & K_{w32} \\ \hline K_{w21} & K_{w22} \end{array}\right]\right)\left\{\begin{array}{c} \{\boldsymbol{\Theta}\} \\ \hline \{\mathbf{q}(-1/2)\} \end{array}\right\} = 0 \tag{37}$$

Equation of motion of a rotating shaft

If we write small amplitude vibration of a rotating shaft around the equilibrium point as

$$e_x = ae^{i\Omega t}\ ,\ e_y = be^{i\Omega t} \tag{38}$$

We may write the equation of motion for the rotating shaft as

$$m\frac{d^2e_x}{dt^2} - f_x = 0 \tag{39}$$

$$m\frac{d^2e_y}{dt^2} - f_y = 0 \tag{40}$$

where *fx* and *fy* denote fluid force acting in the direction of eccentricity and the one of perpendicular direction and *m* denotes mass of a rotating shaft.

Integrating the pressure described by Eq.(29) with enter surface of the rotating shaft, we may obtain fx and fy. Inserting these into Eq.(39) and (40), we finally obtain the equation of a rotating shaft as follows,

$$\left(\left[\begin{array}{cc|cc} J_{R11} & 0 & J_{R12} & 0 \\ 0 & J_{R21} & J_{R22} & 0 \end{array}\right](i\omega)^2 + \left[\begin{array}{cc|cc} 0 & 0 & C_{R11} & C_{R12} \\ 0 & 0 & C_{R21} & C_{R22} \end{array}\right](i\omega) + \left[\begin{array}{cc|cc} 0 & 0 & K_{R11} & K_{R12} \\ 0 & 0 & K_{R21} & K_{R22} \end{array}\right]\right)\left\{\begin{array}{c} \{\mathbf{m}_a\} \\ \{\mathbf{m}_b\} \\ \{\boldsymbol{\Theta}\} \\ \hline \{\mathbf{q}(-1/2)\} \end{array}\right\} = 0. \tag{41}$$

Stability analysis

To start with, we have to combine the equation of motion for the foil and a rotating shaft which yields

$$\left(\left[\begin{array}{cc|cc} J_{R11} & 0 & J_{R12} & 0 \\ 0 & J_{R21} & J_{R22} & 0 \\ \hline 0 & 0 & J_{w31} & 0 \\ 0 & 0 & J_{w21} & 0 \end{array}\right](i\omega)^2 + \left[\begin{array}{cc|cc} 0 & 0 & C_{R11} & C_{R12} \\ 0 & 0 & C_{R21} & C_{R22} \\ \hline 0 & 0 & C_{w31} & C_{w32} \\ 0 & 0 & C_{w21} & C_{w22} \end{array}\right](i\omega) + \left[\begin{array}{cc|cc} 0 & 0 & K_{R11} & K_{R12} \\ 0 & 0 & K_{R21} & K_{R22} \\ \hline 0 & 0 & K_{w31} & K_{w32} \\ 0 & 0 & K_{w21} & K_{w22} \end{array}\right]\right)\left\{\begin{array}{c} \{\mathbf{m}_a\} \\ \{\mathbf{m}_b\} \\ \{\boldsymbol{\Theta}\} \\ \hline \{\mathbf{q}(-1/2)\} \end{array}\right\} = 0 \tag{42}$$

Rewriting the vectors as $\{\boldsymbol{\kappa}_{\mathbf{ma}}\} = (i\omega)\{\mathbf{m}_{\mathbf{a}}\}$, $\{\boldsymbol{\kappa}_{\mathbf{mb}}\} = (i\omega)\{\mathbf{m}_{\mathbf{b}}\}$, $\{\boldsymbol{\kappa}_{\boldsymbol{\Phi}}\} = (i\omega)\{\boldsymbol{\Theta}\}$,then, we have an expression of the conventional form of the dynamical problems as

$$\left(\left[M_a\right](i\omega) - \left[K_a\right]\right)\left\{\begin{array}{c} \{\boldsymbol{\kappa}_{\mathbf{ma}}\} \\ \{\boldsymbol{\kappa}_{\mathbf{mb}}\} \\ \{\boldsymbol{\kappa}_{\boldsymbol{\Phi}}\} \\ \{\mathbf{m}_{\mathbf{a}}\} \\ \{\mathbf{m}_{\mathbf{b}}\} \\ \{\boldsymbol{\Theta}\} \\ \{\mathbf{q}(-1/2)\} \end{array}\right\} = 0\ . \tag{43}$$

where

$$[M_a] = \left[\begin{array}{ccccccc} 0 & 0 & 0 & I & 0 & 0 & 0 \\ 0 & 0 & 0 & 0 & I & 0 & 0 \\ 0 & 0 & 0 & 0 & 0 & I & 0 \\ J_{R11} & 0 & J_{R12} & 0 & 0 & C_{R11} & C_{R12} \\ 0 & J_{R21} & J_{R22} & 0 & 0 & C_{R21} & C_{R22} \\ 0 & 0 & J_{w31} & 0 & 0 & C_{w31} & C_{w32} \\ 0 & 0 & J_{w21} & 0 & 0 & C_{w21} & C_{w22} \end{array}\right] \quad , \quad [K_a] = \left[\begin{array}{ccccccc} I & 0 & 0 & 0 & 0 & 0 & 0 \\ 0 & I & 0 & 0 & 0 & 0 & 0 \\ 0 & 0 & I & 0 & 0 & 0 & 0 \\ 0 & 0 & 0 & 0 & 0 & -K_{R11} & -K_{R12} \\ 0 & 0 & 0 & 0 & 0 & -K_{R21} & -K_{R22} \\ 0 & 0 & 0 & 0 & 0 & -K_{w31} & -K_{w32} \\ 0 & 0 & 0 & 0 & 0 & -K_{w21} & -K_{w22} \end{array}\right]$$

In the following, we performed stability analysis based on complex eigen value analysis.

Calculated results for stability analysis

In Figure 12, results of stability analysis is summarized as a stability diagram where M and Λ denote non-dimensional mass parameter and bearing number defined as

$$M = \frac{mP_a}{2\mu^2 b}\left(\frac{c}{R}\right)^5$$

$$\Lambda = \frac{6\mu\omega}{p_a}\left(\frac{R}{c}\right)^2$$

where $\mu, \omega, R, c, b, p_a$ denote viscosity of the working fluid, rotational angular velocity of the shaft, inner radius of the bearing, clearance between the foil and the surface of the rotating shaft, bearing width and the surrounding pressure, respectively.

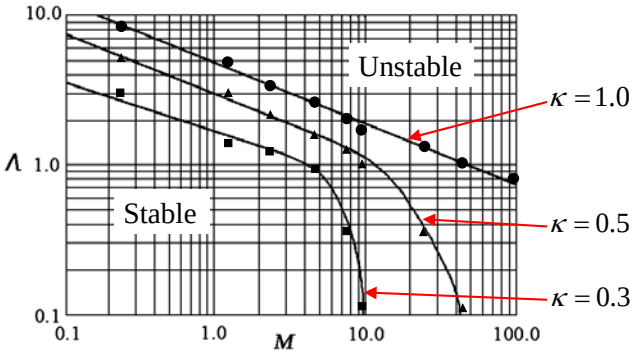

Figure 12 Stability diagram

Major parameters and calculation conditions are shown in Table 1.

Table 1 Bearing specification

Material of foil	phospher bronze
Thickness t_s (m)	2×10^{-4}
Young's modulus E (Pa)	1.10×10^{11}
Density ρ (kg/m^3)	8.78×10^{3}
Diameter of foil bearing R (m)	0.02
Width of foil bearing b (m)	0.02
Radial clearance c (m)	20×10^{-6}
Stiffness of projection k' (N/μm)	0.2

From Figure 12, we can find that unstable area decreases at larger eccenticity ratio and lighter shaft weight which seems to be reasonable.

CONCLUSION

In this study, as a first step to establish design guideline of foil bearings, static and dynamic analyses employing leakage induced vibration theory and discretized beam element method was done and the following results are obtained:

(1) In the static analysis, rotor locus and relationship between eccentricity ratio and load capacity was obtained which explains actually observed tendency that eccentricity may become larger than unity under large deformation of a foil.

(2) In the dynamic analysis, stability diagram was obtained as a function of mass parameter and bearing number which shows that stability can be realized under the condition that light weight, low rotational speed and large initial eccentricity ratio.

REFERENCES

[1] Della Corte, "A New Foil Air Bearing Test Rig for Use to 700℃ and 70,000rpm", Tribology Transactions, 41,3, 335, 1998

[2] DellaCorte, et al., "Steady-State Stiffness of Foil Air Journal Bearings at Elevated Temperatures", Tribology Trans., 44,3, 489, 2001

[3] Hayasi.K., et al., "Development of Aerodynamic Foil Bearing for Small High-speed Rotor", Proc. of 21st Leeds-Lyon Symp. , 291, 1994

[4] Heshmat.H, "Operation of Foil Bearings Beyond the Bending Critical Mode", Transactions of the ASME Journal of Tribology, 122, 192, 2000

[5] Inada F., et al., "A Study on Leakage–Flow-Induced Vibrations, part 1: Fluid–Dynamic Forces and Moments Acting on the Walls of a Narrow Tapered Passage," J. Fluids and Structures, pp. 395-412, 1990.

[6] Kaneko, S., et al., "A Method for Calculating Radial Foil Bearing Characteristics Used for Small-size and High-speed Micro Gas Turbine"Proc.JSME, 04-2, 59, 2004, (in Japanese)

[7] Kaneko S., et al., "Leakage Flow Induced Flutter of Highly Flexible Structures," Proc. 7th International Conference on Flow-Induced Vibration, Lucerne, pp. 811-818, 2000.

[8] Kitazawa, S., et al., Development of Foil Bearing for Micro Gas Turbine Use, IGTC2003Tokyo TS-019, 2003.

[9] Shimizu N., et al., "High speed rotating shaft system supported by air bearing", Honda R&D Technical Review, 15, 2,93,2003, (in Japanese).

[10] Xiaoshan WU, Shigehiko KANEKO, Linear and Nonlinear Analysis of Sheet Flutter Induced by Leakage Flow, Journal of Fluids and Structures 20(8), pp.927-948, 2005

[11] Yabe, H., et al., "Analysis of Basic Characteristics of Air Lubricated Multi Wounded Foil Bearing", Proc. Tribology Conference, Tribology Society of Japan, 299, 2003, (in Japanese).